Effects of hydrodynamic interactions in binary colloidal mixtures driven oppositely by oscillatory external fields

Effects of hydrodynamic interactions in binary colloidal mixtures driven oppositely by oscillatory external fields

Adam Wysocki[1] **and Hartmut Löwen**

Institut für Theoretische Physik II, Heinrich-Heine-Universität Düsseldorf, Universitätsstrasse 1, D-40225 Düsseldorf, Germany

E-mail: adam@thphy.uni-duesseldorf.de and hlowen@thphy.uni-duesseldorf.de

Abstract
The collective dynamics in a binary mixture of colloidal particles which are driven in opposite directions by an external oscillatory field is examined by computer simulations in two spatial dimensions. Both Brownian dynamics (BD) computer simulations, which ignore solvent-mediated hydrodynamic interactions between the colloidal particles, and multi-particle collision dynamics (MPCD) simulations, which include hydrodynamic interactions, are employed. We first review recent results obtained by BD. Depending on the driving frequency and amplitude, lane formation parallel to the drive and band formation perpendicular to the drive occur. Band formation is stable only in a finite window of oscillation frequencies and driving strengths and is taken over by lane formation if the driving force is increased or the oscillation frequency is decreased. MPCD simulations, on the other hand, reveal that band formation is blurred by hydrodynamic interactions. During the front collisions of oppositely driven particles there is a strong vortical movement of the solvent which tends to mix particles and broaden the interface of the bands. This can either lead to a novel intermittent dynamical behaviour or to band rupture into local clusters. These effects, which are absent for BD, are characterized by the strengths of the enstrophy and its spectrum. We finally discuss possible experimental realizations of the models employed.

S Online supplementary data available from stacks.iop.org/JPhysCM/23/284117/mmedia

1. Introduction

Nonequilibrium phase transitions in driven diffusive (dissipative) systems exhibit spatiotemporal pattern formations [8, 2] which are completely different from equilibrium phase transitions. In many cases, an instability of a prepared state hints towards an underlying nonequilibrium phase transition. In particular, it is very intriguing to resolve and follow nonequilibrium dynamics on the particle level, which is possible for mesoscopic colloidal suspensions [21, 22], granular grains [2, 29] or dusty plasmas driven by an external field [26, 37].

For colloidal dispersions, the dynamics is overdamped and quite different from granulates and from dusty plasmas: in granular matter, inelastic collisions play a dominant role [35], while in complex plasmas there is only a small damping of the mesoscopic dust particles [37]. Recent investigations for colloids have considered binary mixtures in constant or time-dependent oscillatory fields which act on the different particle species with a different sign. This can be realized by gravity provided the two particle species have a different buoyant mass [33, 28] or by an electric field [19, 20] if the two particle species have a different charge. In the case of a constant and strong enough drive, lanes of particles driven alike are formed in the direction of the driving field [10, 19, 20]. For a time-dependent oscillatory drive more intriguing behaviour has been discovered. There is a drive-induced ergodicity breaking, see e.g. [7, 25], or axial segregation. In the latter case, colliding bands of species driven alike are formed perpendicular to the driving field [39], which is also observed in shaken or vibrated granular systems [27, 34, 3].

---

[1] Present address: Theoretical Soft Matter and Biophysics, Institute of Complex Systems, Forschungszentrum Jülich, Jülich 52425, Germany.
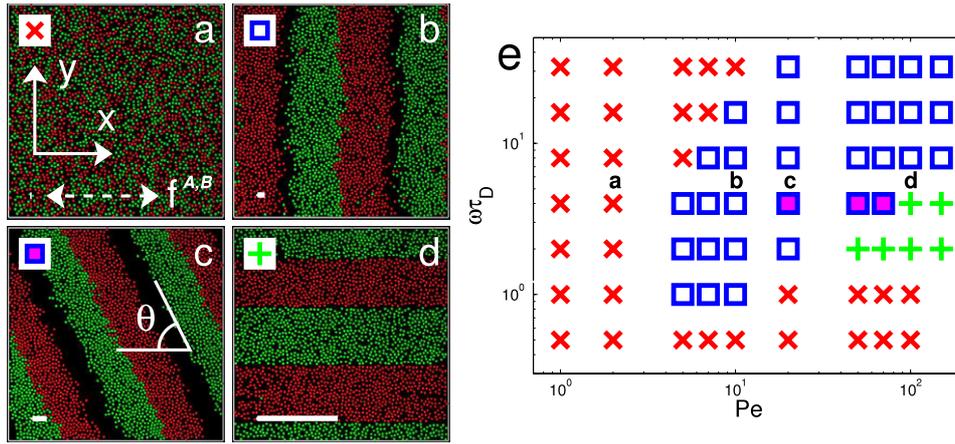
Figure 1. ((a)–(d)) Brownian dynamics simulation snapshots for fixed driving frequency $\omega\tau_D = 4$ and different Peclet numbers Pe after 10^4 periods starting from a fully mixed configuration. The light grey particles are of species A while the dark grey particles are of species B. The symbols in the left upper corner correspond to symbols used in (e). In (a) the coordinate frame is shown and the direction of the driving field is indicated by the broken arrow. In (a)–(d) the lengths of the solid bars (bottom left corner) correspond to the peak-to-peak amplitude of a free particle driven without noise in the external field. For small Pe, we observe a disordered state (a), for intermediate Pe colloids segregate into stripes oriented perpendicular or tilted (tilt angle θ) to the direction of the oscillating force ((b)–(c)); on the other hand, for high Pe, lanes are formed parallel to the direction of the oscillatory force (d). The parameters are $\omega\tau_D = 4$ and $Pe = 2, 10, 20, 110$ from (a) to (d). (e) Nonequilibrium steady state phase diagram for fixed area fraction $\phi = 0.4$. From [39].

In this paper, we explore band formation in oscillatory binary colloidal mixtures by computer simulations. We first review previous work [39] where Brownian dynamics simulations were used which ignore hydrodynamic interactions. The nonequilibrium steady state phase diagram as a function of driving strength and frequency involves both bands and lanes. Furthermore, by increasing the magnitude of the driving force or decreasing the oscillation frequency, the system gets back either to a disordered state or to lane formation with an intermediate regime where mixing of segregation and tilted lanes occurs. Decreasing the magnitude of the driving or increasing the oscillation frequency, on the other hand, always yields a disordered steady state. We then present new results using multi-particle collision dynamics (MPCD) simulations which generate hydrodynamic interactions between colloidal particles. The MPCD simulations reveal that band formation is blurred by hydrodynamic interactions. During the front collisions of oppositely driven particles massive swirls in the solvent velocity field are created which tend to mix particles and broaden the interface of the bands. They can even destroy the banded structure leading to a novel intermittency where bands are formed and destroyed on a timescale much larger than the driving periodicity. We characterize these effects by the strengths of the enstrophy and its spectrum. Finally we briefly discuss possible experimental realizations of the driven colloidal system.

2. Band formation in oscillatory driving fields without hydrodynamic interactions

In Brownian dynamics (BD), the time evolution of the individual colloids is governed by completely overdamped Langevin equations with thermal noise [1]. The particles of sorts A and B are subjected to an oscillatory inversely phased

force $\mathbf{f}^A(t) = -\mathbf{f}^B(t) = f_0 \sin(\omega t)\mathbf{e}_x$, where ω is the driving frequency and f_0 the driving strength. A single particle will follow a noise-averaged trajectory which is sinusoidal in time with an amplitude $f_0/(\xi\omega)$, where ξ is the friction constant. In this approach the friction constants are position-independent and therefore solvent-mediated hydrodynamic interactions are neglected.

We review briefly results from [39]. A two-dimensional equimolar binary mixture of $N = 2864$ hard discs of diameter σ was simulated in a square of size $L = 75\sigma$ with periodic boundary conditions at a total area fraction $\phi = N/L^2\pi(\sigma/2)^2 = 0.4$. It is convenient to define the Peclet number $Pe = f_0\sigma/(2k_BT) = \tau_D/\tau_d$ as a reduced measure for the driving strength. The Peclet number is the ratio between the time $\tau_D = \sigma^2/(4D)$ it takes a colloid to diffuse over its own radius and the time $\tau_d = \sigma/(2v_d)$ it takes to drift the same distance under the action of a constant external force f_0. Here $D = k_BT/\xi$ denotes the short-time diffusion constant, where k_BT is the thermal energy and $v_d = f_0/\xi$ is the maximal drift velocity.

The initial configuration of the BD simulation was an equilibrated fully mixed configuration as realized in the absence of the drive. At time $t = 0$, the oscillatory force is turned on instantaneously and the evolution of the system is followed by using a finite time-step algorithm [1] up to about 10^5 oscillation cycles. Depending on the Peclet number Pe and the reduced frequency $\omega\tau_D$, the system ends up in different steady states constituting the dynamical response of the system to the drive.

The nonequilibrium steady state phase diagram obtained is shown in figure 1, spanning two decades in both driving frequency $\omega\tau_D$ and strength Pe. For very low driving strengths, the external drive is not strong enough to generate order in the completely mixed equilibrium state, leading to a disordered steady state which is depicted in a typical snapshot

in figure 1(a). As visible in figure 1(a), the disordered state can possess an intrinsic finite correlation length as set by colliding clusters which is larger than the interparticle distance, but these structures do not span the whole simulation box. For very high frequencies, on the other hand, a free particle would just perform oscillations with a very small amplitude due to the drive. This amplitude v_d/ω is indicated by a bar in the corresponding simulation snapshots in figures 1(a)–(d). Therefore, at high frequencies, an ensemble of many particles is rattling over a small distance and is thus not perturbing much the disordered equilibrium state. On the other hand, at very low frequencies and at a critical Pe, lane formation similar to that observed earlier for a static field [10, 4, 5, 32] occurs where the direction of the lanes coincides with the drive direction. A corresponding simulation snapshot is given in figure 1(d).

In a region of finite frequencies ($\omega\tau_D > 1$) and Peclet numbers ($Pe > 1$), bounded by disordered and laned steady states, band formation shows up, where the stripes are oriented perpendicular to the drive direction. This is depicted in the corresponding snapshot in figure 1(b). Here the particles driven alike perform oscillations collectively as induced by the external drive but collide periodically with an opposing band of opposite particles. It is important to note here that the interface of the bands is sharp and the separation between oppositely driven particles is almost complete. Moreover, once bands are formed they are pretty robust against fluctuations in the finite system and stay stable within the timescale of the simulation. In the thermodynamic limit, the system is expected to coarsen *ad infinitum*. Finally, in a subregion of axial segregation, some steady states are observed with tilted bands. A snapshot of tilted bands with tilt angle θ relative to the drive direction is shown in figure 1(c).

There are reentrant effects of the disordered phase in figure 1(e): first, by increasing the Peclet number at fixed frequency $\omega\tau_D \approx 1$, the steady state transforms from the disordered one into bands and back to the disordered one. Second, now for increasing frequency at fixed Peclet number $5 < Pe < 10$, the disordered phase is taken over by the banded phase and then appears again.

3. Band formation in oscillatory driving fields with hydrodynamic interactions

3.1. The simulation model

We now extend our simulation technique to account for hydrodynamic interactions by using MPCD. In detail, our two-dimensional system consists of a suspension of N solute particles with mass M and hard disc diameter σ immersed in a bath of N_s solvent particles with mass m and a number density $n_s = N_s/L^2$, where L^2 is the area of the simulation box with periodic boundary conditions in both directions. The N colloidal particles with space position $\mathbf{R}_i$ and velocity $\mathbf{V}_i$ propagate according to Newton's equation of motion

$$M \frac{d\mathbf{V}_i}{dt} = \mathbf{F}^\alpha(t) - \sum_{j \neq i} \nabla_{\mathbf{R}_j} V(R_{ij}). \quad (1)$$

The first term on the right-hand side represents the oscillatory driving force of strength f_0 directed along the y-axis with the

driving frequency $\omega = 2\pi/T$ (T is period). This force is inversely phased for particles of sorts A and B, i.e. $\mathbf{F}^A(t) = -\mathbf{F}^B(t) = f_0 \sin(\omega t)\mathbf{e}_y$. The second one represents the force due to the interaction with other colloids ($R_{ij} = |\mathbf{R}_i - \mathbf{R}_j|$ is the interparticle distance). To avoid overlap the colloids interact via a screened Coulomb potential which diverges at $R_{ij} = \sigma$. The reduced inverse screening length is set to $\kappa\sigma = 16$. We integrate the equation of motion using a velocity Verlet algorithm with a time step δt. Simultaneously, the solvent particles with space position $\mathbf{r}_i$ and velocity $\mathbf{v}_i$ move ballistically also within the same time step δt, i.e.

$$\mathbf{r}_i(t + \delta t) = \mathbf{r}_i(t) + \mathbf{v}_i(t)\delta t. \quad (2)$$

To enforce the no-slip boundary condition on the colloid surface a stochastic reflection method [17, 30, 38] is applied. If a solvent particle i hits a colloid it gets a new velocity $\mathbf{u}_i = \mathbf{u}_{n,i} + \mathbf{u}_{t,i}$ relative to the velocity of the colloid's boundary from a distribution for the normal velocity component

$$P_n(u_n) = \frac{mu_n}{k_B T} \exp\left(-\frac{mu_n^2}{2k_B T}\right) \quad (3)$$

and the tangential velocity component

$$P_t(u_t) = \left(\frac{m}{2\pi k_B T}\right)^{1/2} \exp\left(-\frac{mu_t^2}{2k_B T}\right). \quad (4)$$

Then the new velocity of the solvent particle i after collision with the colloid j reads as

$$\mathbf{v}_i(t + \delta t) = \mathbf{V}_j(t) + \mathbf{\Omega}_j(t) \times (\mathbf{r}_i' - \mathbf{R}_j(t)) + \mathbf{u}_i, \quad (5)$$

where $\mathbf{\Omega}_j$ is the angular velocity of the colloid and $\mathbf{r}_i'$ is the point of contact at the colloid surface. After all collisions within δt are completed, the new velocity of the colloid j is updated as

$$\mathbf{V}_j(t + \delta t) = \mathbf{V}_j(t) + \frac{m}{M} \sum_{i \in \mathcal{C}} (\mathbf{v}_i(t) - \mathbf{v}_i(t + \delta t)) \quad (6)$$

and the new angular velocity is

$$\mathbf{\Omega}_j(t + \delta t) = \mathbf{\Omega}_j(t) + \frac{m}{I} \sum_{i \in \mathcal{C}} (\mathbf{r}_i' - \mathbf{R}_j(t))$$
$$\times (\mathbf{v}_i(t) - \mathbf{v}_i(t + \delta t)), \quad (7)$$

where $\mathcal{C}$ is the set of solvent particles colliding with colloid j within the time interval $[t, t + \delta t]$ and $I = \frac{1}{2}M(\frac{\sigma}{2})^2$ is the moment of inertia of a solid disc.

After a time $\Delta t = n\delta t$ the solvent particles interact with each other via a multi-particle collision [24]. The particles are sorted in square cells of size a and the centre-of-mass velocity $\mathbf{U}_\xi = N_\xi^{-1} \sum_{j \in \xi} \mathbf{v}_j$ of each cell ξ is calculated (N_ξ is the number of particles in the cell ξ). Then in each cell the relative velocities $\delta\mathbf{v}_i = \mathbf{v}_i - \mathbf{U}_{\xi_i}$ are rotated by an angle α around a random axis, i.e.

$$\mathbf{v}_i(t + \Delta t) = \mathbf{U}_{\xi_i}(t) + S_{\xi_i} \mathsf{R}_{\xi_i}(\alpha)\delta\mathbf{v}_i(t), \quad (8)$$

where $\mathsf{R}_{\xi_i}(\alpha)$ is the stochastic rotation matrix and S_{ξ_i} is a thermostat operator (see below). $\mathsf{R}_{\xi_i}(\alpha)$ is equal for

all particles within the same cell but uncorrelated between different cells and in time. Due to this operation the particles exchange momentum in the cell while the total kinetic energy and the total momentum in the cell are conserved. It was shown [24] that (2) and (8) lead in equilibrium to a Maxwell–Boltzmann distribution of the velocities and that Navier–Stokes hydrodynamics is generated.

Since in any kind of nonequilibrium simulation thermostating is required to avoid viscous heating, we rescale the relative velocities $\delta \mathbf{v}_i$ in each cell by a factor

$$S_\xi = \left[2(N_\xi - 1)k_{\mathrm{B}}T \left(m \sum_{i \in \xi} \delta \mathbf{v}_i^2 \right)^{-1} \right]^{1/2}. \qquad (9)$$

This thermostat acts locally and is unbiased with respect to the flow field; hence it does not destroy the hydrodynamic behaviour, see [13].

For small mean free path $\lambda = \Delta t \sqrt{m/(k_{\mathrm{B}}T)} \ll a$ the same set of particles interact over several Δt with each other before leaving this cell and hence they remain correlated over several Δt. If one imposes a flow field the degree of correlation and therefore the transport coefficients depend on the direction and on the magnitude of the flow field. The violated Galilean invariance can be restored if all particle positions are shifted by a random vector before the collision step [16].

We employed the parameters $\Delta t = \delta t = 0.025\tau$, $\alpha = \pi/2$, $n_s a^2 = 5$, with $\tau = \sqrt{ma^2/(k_{\mathrm{B}}T)}$. With these parameters the total solvent kinematic viscosity is $\nu = \eta/\rho \approx 2.67 a^2/\tau$ ($\rho = mn_s$ is the mass density and η the dynamic viscosity) [18]. Our simulation box with dimension $L = 120\sigma$ contains $N = 2750$ colloids with mass $M = 63m$ and hard core diameter $\sigma = 4a$; the total area fraction is $\phi = 0.15$. Within a finite time window of about 450τ (maximum period considered is $T = 428\tau$), we calculate the translational diffusion constant from the integral of the velocity autocorrelation function and obtain $D \approx 0.0273 a^2/t_0$ [30]. With these parameters we achieve nearly the hierarchy of timescales for a colloidal particle $\Delta t = 0.025\tau \ll \tau_c = 1.4\tau < \tau_\nu = 1.5\tau < \tau_B = 1.7\tau \ll \tau_{\mathrm{D}} = 146\tau$, see [31]. Here τ_c is the time a sound wave needs to propagate over one colloidal radius (the speed of sound is $c = \sqrt{2k_{\mathrm{B}}T/m}$), τ_B is the time the velocity of a colloid is correlated and τ_ν is the time over which the solvent momentum diffuses over one colloidal radius. We performed simulations at $Pe = 10$, which corresponds to a Reynolds number of $Re = D/\nu Pe \approx 0.1 < 1$, such that inertial effects are negligible. To avoid compressibility effects we also ensure that the Mach number is smaller than unity, $Ma = 2D/(\sigma c)Pe = 0.1 < 1$. With these values of the hydrodynamic numbers and the hierarchy of timescales we are sure that a comparison with a real physical system is reasonable. Still one has to be careful about compressibility effects and collective sound waves, in particular if a periodic drive is applied.

3.2. Results

For fixed Peclet number $Pe = 10$, we show simulation data for three different driving frequencies $\omega\tau_{\mathrm{D}} = 2.1$ (run A), $\omega\tau_{\mathrm{D}} =$ 3.2 (run B) and $\omega\tau_{\mathrm{D}} = 6.4$ (run C). In figure 2 (left column), simulation snapshots of the driven particles are shown after a long initialization time (corresponding to about 400–1000 cycles) starting from a completely mixed configuration. The coarse-grained solvent velocity field $\mathbf{v}(\mathbf{r})$ is indicated by arrows. Simultaneously, the corresponding vorticity field of the solvent velocity which is defined as $\nabla \times \mathbf{v}(\mathbf{r})$ is shown in the right column (in units of τ^{-1}). Here the coarse-grained solvent velocity $\mathbf{v}(\mathbf{r})$ is a mean over 8^2 MPCD collision cells. In two spatial dimensions, the vorticity field has only one component and its strength is shown in a grey-scale code (online colour code). Movies corresponding to the snapshots in figure 2 are provided in the supplementary information (available as movies 1–3 at stacks.iop.org/JPhysCM/23/284117/mmedia). In order to facilitate a direct comparison between BD and MPCD, we have included plots showing snapshots in the steady state of the BD simulation in figures 2(c), (f) and (i). The BD simulations are carried out for the same parameters ϕ, Pe and $\omega\tau_{\mathrm{D}}$ as the MPCD.

Clearly, in run A, the system is in a banded steady state, see figure 2(a). The front of the bands is, however, much more disordered than it is without hydrodynamic interactions (see figure 2(c)) where the particle species are clearly demixed and segregated.

Concomitantly, during the front collision of oppositely driven bands, there is a clear vortex formation in the solvent velocity, see figure 2(b). The swirl intensity is pronounced if particle bands are colliding. Intuitively this has to do with the fact that colliding bands get unstable, similar to Rayleigh–Taylor instability, so that growing undulations of the interface between particles of oppositely driven species induce vortices in the fluid due to momentum conservation. There is a second interface between oppositely driven particles which is rougher and situated at the bottom of figure 2(a). This describes the locations where different particles are driven away from each other. Also close to this interface there is a strong tendency to form swirls.

If the driving frequency is growing (figure 2(d)), bands become local and do not span the whole system. Instead there are clusters of particles driven alike which involve many particles. This is in complete contrast to BD where the configuration is disordered and such large clusters are missing (see the corresponding snapshots in figure 2(i)). Again there is a massive swirling concomitant with the cluster collisions, as indicated by the high value for the velocity curl field which is vanishing in BD.

In figure 3(a) we have started an MPCD simulation using the parameters of run A from a banded state generated by BD simulations; this configuration is identical to that of figure 2(c). While this banded configuration is by construction stable in the BD case, hydrodynamic interactions cause the band to break (figures 3(a)–(d)) by a mechanism reminiscent of a Rayleigh–Taylor instability [40] (see also movie 4 in the supporting information available at stacks.iop.org/JPhysCM/23/284117/mmedia). More interestingly, after about ten cycles there are bands again. The MPCD banded state, however, differs qualitatively from the BD banded state since it exhibits an intermittency [36], i.e. bands are forming and dissolving on
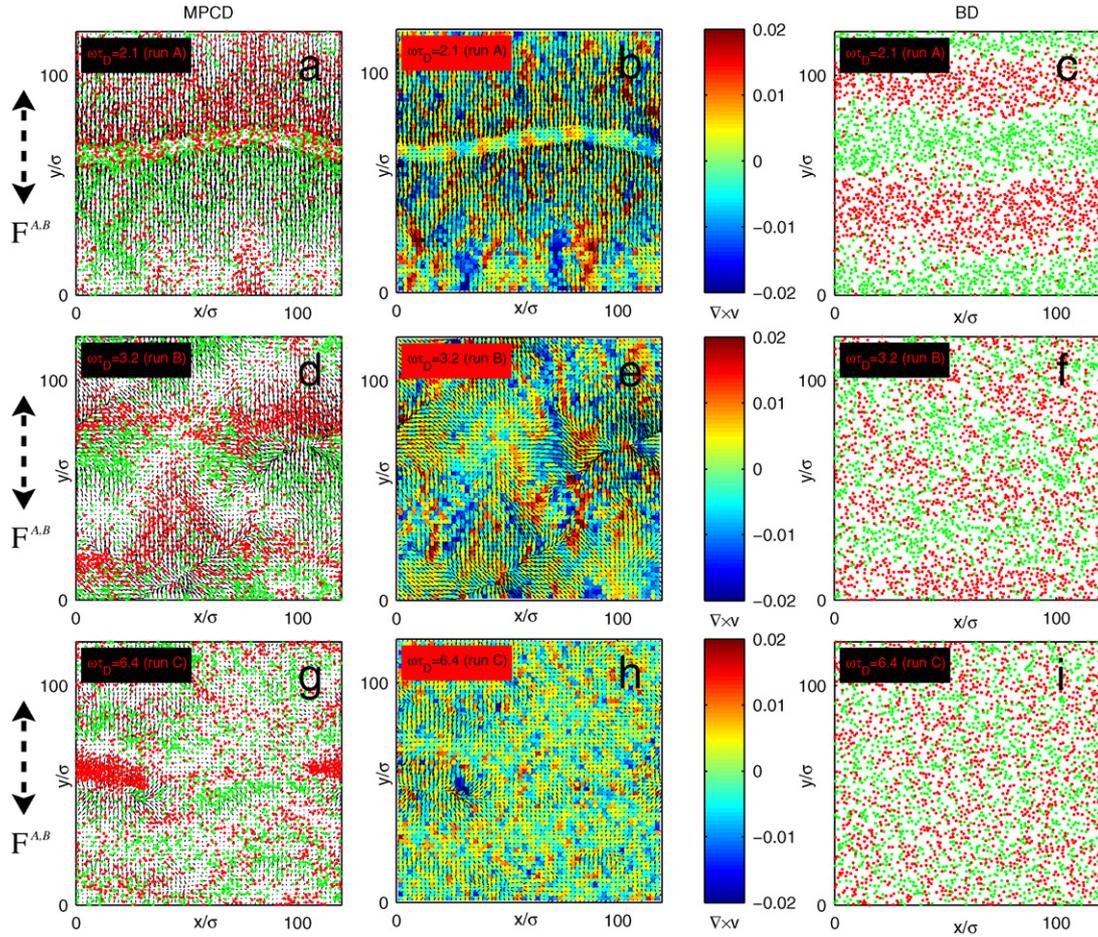
Figure 2. ((a)–(i)) Snapshots of run A ($\omega\tau_D = 2.1$), run B ($\omega\tau_D = 3.2$) and run C ($\omega\tau_D = 6.4$) in the steady state. The system initiates from a completely mixed configuration. The oscillatory driving force acts along the y-axis (broken arrow). The left column ((a), (d), (g)) displays MPCD simulation snapshots (particles of sort A are in red, while particles of sort B are in green) together with the coarse-grained solvent velocity field $\mathbf{v}(\mathbf{r})$ (black arrows). The middle column ((b), (e), (h)) corresponds to the left column and illustrates the solvent velocity field $\mathbf{v}(\mathbf{r})$ (black arrows) and the corresponding vorticity field $\nabla \times \mathbf{v}(\mathbf{r})$ in units of τ^{-1} (colour coded). Parts (a) and (b) show the situation at time $t/T = 650.25$, (d) and (e) at time $t/T = 1000.25$, and (g) and (h) at time $t/T = 1900.25$. See also movies 1–3 in the supporting information available at stacks.iop.org/JPhysCM/23/284117/mmedia. The right column ((c), (f), (i)) is the same as ((a), (d), (g)) but now for BD computer simulations. Part (c) is at $t/T = 4500.25$, (f) is at $t/T = 6500.25$ and (i) is at $t/T = 9500.25$.

a timescale larger than the drive period, an effect which will be addressed below.

In order to characterize the averaged degree of swirling we have calculated the time dependence of the enstrophy $\mathcal{S}$ of the solvent velocity field as defined by

$$\mathcal{S} = \frac{1}{2} \int_A |\nabla \times \mathbf{v}|^2 \mathrm{d}^2 \mathbf{r}. \tag{10}$$

This quantity is plotted in figure 3(e) as a function of time. While the enstrophy is oscillating with the external driving frequency, the initial instability of the banded state is accompanied with a peak at small times indicating a strong mixing in the first few periods.

More data for the enstrophy are shown on a longer timescale in figure 4(a) for all three runs. There is a high degree of swirling in all three cases shown. In the Brownian case, clearly $\mathcal{S} = 0$. However, while for run A strong spikes are visible, this is much less pronounced for runs B and C. After a long initialization time, i.e. in the steady state, we start

to measure the enstrophy $\mathcal{S}(t)$ at $N = 16\,385$ points in time using a sampling interval of $\Delta t = T/32$; the corresponding observation time is $(N-1)\Delta t = 512T$. The discrete Fourier transform of $\mathcal{S}(t_j)$ reads as

$$\hat{\mathcal{S}}(\tilde{\omega}_k) = \sum_{j=0}^{N-1} \mathcal{S}(t_j) \exp\left(-2\pi \mathrm{i} jk/N\right) \qquad k = 0, \ldots, N-1 \tag{11}$$

with discrete frequencies $\tilde{\omega}_k = 2\pi k/N\Delta t$ and discrete times $t_j = j\Delta t$.

Its power spectrum $\frac{|\hat{\mathcal{S}}|^2}{N^2}(\tilde{\omega})$ is plotted in figure 4(b) as a function of frequency $\tilde{\omega}$; the power spectra are averages of four independent simulation runs. For all runs, there are frequency peaks at the driving frequency and its multiples (i.e. when $\tilde{\omega} = n\omega$ with $n = 1, 2, 3, \ldots$), which clearly show the periodicity of the drive and its nonlinear higher-order harmonic generations. Interestingly, the even multiples have a stronger weight in the power spectrum than the odd ones, an effect which remains to be explained.
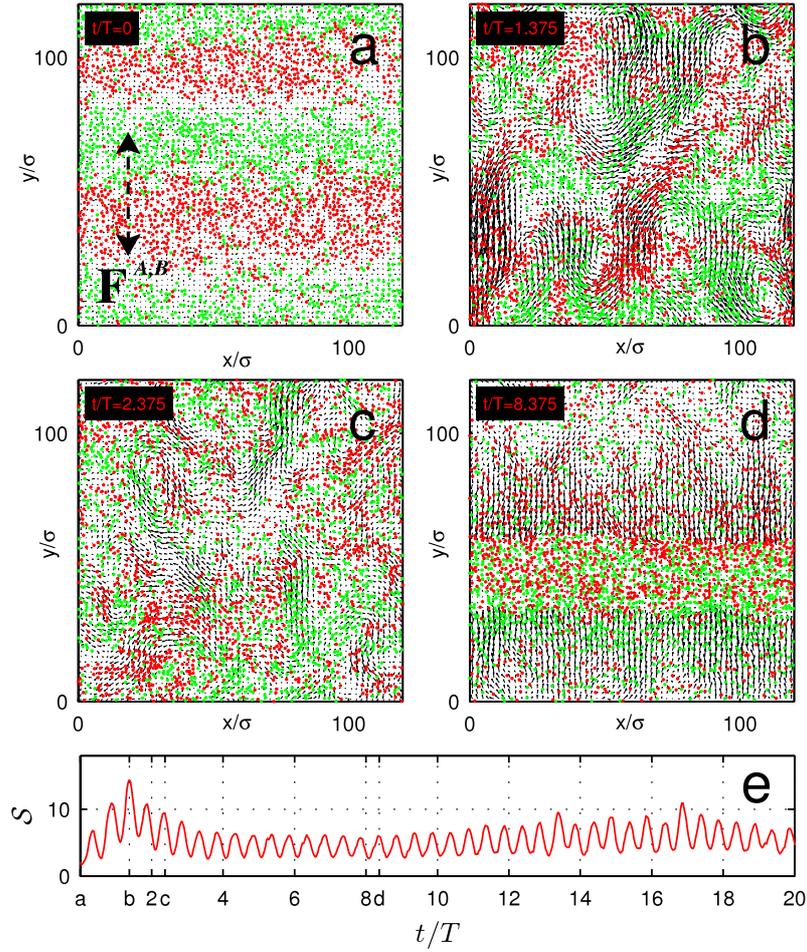
Figure 3. ((a)–(e)) Time evolution of an unstable segregated system using a simulation which includes hydrodynamic interactions (MPCD). Here the initial configuration of the MPCD simulation was a segregated particle setup which was generated with a BD simulation after 5000 periods of oscillation. The parameters in MPCD as well as in BD are those of run A, i.e. $Pe = 10$ and $\omega\tau_D = 2.1$. ((a)–(d)) Particle configuration together with the coarse-grained solvent velocity field $\mathbf{v}(\mathbf{r})$ (black arrows) at time $t/T = 0$ (a), $t/T = 1$ (b), $t/T = 2$ (c) and $t/T = 8$ (d). The oscillatory driving force acts along the y-axis (broken arrow). The time evolution of the enstrophy $\mathcal{S} = \frac{1}{2}\int_A |\nabla \times \mathbf{v}|^2\, d^2\mathbf{r}$ is shown in (e). See also movie 4 in the supporting information available at stacks.iop.org/JPhysCM/23/284117/mmedia.
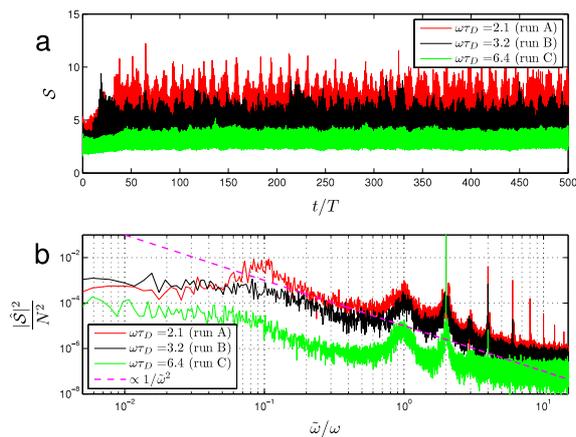
Figure 4. (a) Time dependence of the enstrophy $\mathcal{S} = \frac{1}{2}\int_A |\nabla \times \mathbf{v}|^2\, d^2\mathbf{r}$ belonging to the solvent velocity field $\mathbf{v}(\mathbf{r})$ for run A, B and C. The time is normalized by the corresponding driving period $T = 2\pi/\omega$. (b) Log–log plot of the power spectrum $|\hat{\mathcal{S}}|^2/N^2$ of the enstrophy $\mathcal{S}$ versus the frequency $\tilde{\omega}$. $\hat{\mathcal{S}}(\tilde{\omega})$ is the Fourier transform of $\mathcal{S}$ and $\tilde{\omega}$ is normalized by the corresponding driving frequency ω. The dashed line indicates an inverse quadratic scaling of the spectrum, i.e. $|\hat{\mathcal{S}}|^2 \propto 1/\tilde{\omega}^2$.

For lower frequencies the power spectrum scales with the inverse square frequency, $|\hat{\mathcal{S}}|^2 \propto 1/\tilde{\omega}^2$; note the double logarithmic plot of figure 4(b). Such a Lorentzian power spectrum is ubiquitous in processes with exponential relaxations [6]. More interestingly, there is an additional low-frequency peak at about $\omega/10$ for run A which is a clear signature of the intermittent behaviour of banding. For runs B and C, on the other hand, there is no such low-frequency peak in the power spectrum. We conclude, therefore, that hydrodynamic interactions can cause intermittency in driven colloidal systems at low Reynolds numbers.

4. Conclusions and experimental realizations

In conclusion, we have shown that two species of oscillatory driven colloids can segregate into stripes perpendicular to the drive for appropriate frequencies and driving strengths. The effect is altered if hydrodynamic interactions are added. The latter induce swirls at the interface of oppositely driven particles. We find two possibilities for the thermodynamic state for hydrodynamic interactions: either it shows a laterally

system-spanning band which is accompanied by a novel intermittent behaviour or the bands rupture into local clusters. Since we have studied a two-dimensional model, the effect of hydrodynamic interactions is somehow maximized. In a three-dimensional system confined to a slit, the effects induced by hydrodynamic interactions are expected to be less pronounced.

In principle, it is possible to verify banding in real-space experiments on driven binary colloidal mixtures. Experimental realizations are superparamagnetic colloids driven by a gradient in a magnetic field [12], oppositely charged colloidal mixtures exposed to an alternating electric field [19, 20], colloids driven by gravity [12, 33] in a rotating cell or colloidal mixtures driven by dielectrophoretic force in a nonuniform ac electric field [41]. In particular, oppositely charged colloids in an ac electric field are a very promising realization. As a side remark, however, the jamming in bands perpendicular to the field discussed in [19, 20] is different from banding, since a constant (i.e. time-independent) electric field was applied. If an electric field is applied, hydrodynamic interactions are strongly screened [23], while they are fully developed for gravity [32].

In future work, we plan to explore the influence of hydrodynamic interaction on other than banded states (laned, tilted) for an oscillatory drive. Also the three-dimensional case needs to be explored, in particular, if hydrodynamic interactions are included. They can be included either by MPCD simulations in three dimensions [40] or by applying the appropriate hydrodynamic mobility tensors [32]. It would also be interesting to explore higher densities where freezing occurs [11]. An external oscillating field would then lead to particle rattling in the cages [14, 9], which can efficiently melt the crystal [15].

Acknowledgments

References

[1] Allen M P and Tildesley D J 1991 *Computer Simulation of Liquids* (Oxford: Oxford University Press) p 263
[2] Aranson I S and Tsimring L S 2006 *Rev. Mod. Phys.* **78** 641
[3] Ciamarra M P, Coniglio A and Nicodemi M 2005 *Phys. Rev. Lett.* **94** 188001
[4] Chakrabarti J, Dzubiella J and Löwen H 2003 *Europhys. Lett.* **61** 415
[5] Chakrabarti J, Dzubiella J and Löwen H 2004 *Phys. Rev.* E **70** 012401
[6] Coffey W T, Kalmykov Yu P and Waldron J T 2003 *The Langevin Equation with Applications to Stochastic Problems in Physics, Chemistry, and Electrical Engineering* (Singapore: World Scientific) p 241
[7] Corte L, Chaikin P M, Gollub J P and Pine J P 2008 *Nature Phys.* **4** 420
[8] Cross M C and Hohenberg P C 1993 *Rev. Mod. Phys.* **65** 851
[9] Das M, Ananthakrishna G and Ramaswamy S 2003 *Phys. Rev.* E **68** 061402
[10] Dzubiella J, Hoffmann G P and Löwen H 2002 *Phys. Rev. E* **65** 021402
[11] Dzubiella J and Löwen H 2002 *J. Phys.: Condens. Matter* **14** 9383
[12] Erbe A, Zientara M, Baraban L, Kreidler C and Leiderer P 2008 *J. Phys.: Condens. Matter* **20** 404215
[13] Evans D J and Morriss G P 1986 *Phys. Rev. Lett.* **56** 2172
[14] Löwen H and Hoffmann G P 1999 *Phys. Rev.* E **60** 3009
[15] Hoffmann G P and Löwen H 2000 *J. Phys.: Condens. Matter* **12** 7359
[16] Ihle T and Kroll D M 2001 *Phys. Rev.* E **63** 020201
[17] Inoue Y, Chen Y and Ohashi H 2002 *J. Stat. Phys.* **107** 85
[18] Kikuchi N, Pooley C M, Ryder J F and Yeomans J M 2003 *J. Chem. Phys.* **119** 6388
[19] Vissers T, Wysocki A, Rex M, Löwen H, Royall C P, Imhof A and van Blaaderen A 2011 *Soft Matter* **7** 2352
[20] Leunissen M E, Christova C G, Hynninen A-P, Royall C P, Campbell A I, Imhof A, Dijkstra M, van Roij R and van Blaaderen A 2005 *Nature* **437** 235
[21] Löwen H 2001 *J. Phys.: Condens. Matter* **13** R415
[22] Löwen H 2010 *Soft Matter* **6** 3133
[23] Long D and Ajdari A 2001 *Eur. Phys. J.* E **4** 29
[24] Malevanets A and Kapral R 1999 *J. Chem. Phys.* **110** 8605
[25] Mangan N, Reichhardt C and Reichhardt C J O 2008 *Phys. Rev. Lett.* **100** 187002
[26] Morfill G E and Ivlev A V 2009 *Rev. Mod. Phys.* **81** 1353
[27] Mullin T 2000 *Phys. Rev. Lett.* **84** 4741
[28] Okubo T, Okamoto J and Tsuchida A 2008 *Colloid Polym. Sci.* **286** 1123
[29] Ottino J M and Khakhar D V 2000 *Annu. Rev. Fluid Mech.* **32** 55
[30] Padding J T, Wysocki A, Löwen H and Louis A A 2005 *J. Phys.: Condens. Matter* **17** S3393
[31] Padding J T and Louis A A 2006 *Phys. Rev.* E **74** 031402
[32] Rex M and Löwen H 2008 *Eur. Phys. J.* E **26** 143
[33] Royall C P, Dzubiella J, Schmidt M and van Blaaderen A 2007 *Phys. Rev. Lett.* **98** 188304
[34] Sánchez P, Swift M R and King P J 2004 *Phys. Rev. Lett.* **93** 184302
[35] Kranz W T, Sperl M and Zippelius A 2010 *Phys. Rev. Lett.* **104** 225701
[36] Sreenivasan K R and Antonia R A 1997 *Annu. Rev. Fluid Mech.* **29** 435
[37] Sütterlin K R *et al* 2009 *Phys. Rev. Lett.* **102** 085003
[38] Whitmer J K and Luijten E 2010 *J. Phys.: Condens. Matter* **22** 104106
[39] Wysocki A and Löwen H 2009 *Phys. Rev.* E **79** 041408
[40] Wysocki A, Royall C P, Winkler R G, Gompper G, Tanaka H, van Blaaderen A and Löwen H 2009 *Soft Matter* **5** 1340
[41] Zhao J, Vollmer D, Butt H J and Auernhammer G K 2008 *J. Phys.: Condens. Matter* **20** 404212